AJNR

The extracranial facial nerve: high resolution three-dimensional Fourier transform MR imaging.

R B McGhee, Jr, D W Chakeres, P Schmalbrock, M A Brogan and J A Negulesco

AJNR Am J Neuroradiol 1993, 14 (2) 465-472
http://www.ajnr.org/content/14/2/465

The Extracranial Facial Nerve: High Resolution Three-Dimensional Fourier Transform MR Imaging

Robert B. McGhee, Jr.,[1,3] Donald W. Chakeres,[1] Petra Schmalbrock,[1] Martha A. Brogan,[1] and John A. Negulesco[2]

PURPOSE: To investigate the use of high-resolution three-dimensional Fourier transform gradient-echo MR in evaluation of the extracranial facial nerve. **METHODS:** Nine normal subjects and one clinical patient were scanned. Several imaging parameters, including echo time, field-of-view, and the use of Gd-DTPA, were manipulated to determine the optimal technique. Adequate results were obtained in less than 7 minutes acquisition time using a T1-weighted (50/5.3) gradient-echo technique, with a 30° flip angle, a 12-cm field of view, 128 × 256 matrix, and 28 or 60 1.0-mm-thick contiguous sections. **RESULTS:** Gd-DTPA administration was not found useful in identifying the normal extracranial facial nerve. The proximal extracranial facial nerve was seen as a branching low signal intensity tubular structure on 10 to 20 contiguous images in all five volunteers in which this optimal technique was employed. Postprocessing of the images to produce curved oblique planar reconstructed images was useful to display long segments of the facial nerve on a single image. **CONCLUSION:** Our experience with high resolution three-dimensional Fourier transform MR imaging indicates that it can consistently demonstrate the intraparotid facial nerve on multiple contiguous images.

Index terms: Neck, anatomy; Face, magnetic resonance; Nerves, magnetic resonance; Nerves, facial (VII)

AJNR 14:465–472, Mar/Apr 1993

Facial nerve dysfunction is a common clinical problem that often requires imaging techniques to determine the nature of the abnormality (1, 2). Because facial nerve dysfunction may be related to abnormalities anywhere from the contralateral cerebral hemisphere to peripheral branches of the facial nerve in the superficial soft tissues of the face, it is extremely helpful to localize the area of possible abnormality using history and clinical findings. Once the level of possible abnormality has been localized clinically, the best imaging modality for that region can be chosen.

The use of standard two-dimensional Fourier transform (2DFT) thick-section magnetic resonance (MR) imaging to evaluate the extracranial facial nerve has been reported (3–5), but has many limitations. Minimum section thickness is limited to approximately 3 mm using conventional 2DFT spin-echo sequences, due to gradient strength limitations and decreasing signal-to-noise ratio with thinner sections. An additional intersection gap to minimize cross talk is usually necessary. The extracranial facial nerve may be seen using these conventional 2DFT spin-echo techniques, but is typically seen only on one to three images (3). Because of the small size and complex anatomy of the intraparotid facial nerve and surrounding structures, increased spatial resolution would provide more accurate information on the appearance of the nerve and its relationship to adjacent pathology.

An additional difficulty of conventional 2DFT spin-echo techniques is the similarity in signal between the facial nerve and vascular structures. Because both are seen as low-signal tubular struc-

Received January 29, 1992; revision requested April 21; revision received June 15 and accepted July 21.

This work was supported by a grant from General Electric Medical Systems.

[1] Department of Radiology, Division of Neuroradiology, Ohio State University Hospitals, Ohio State University College of Medicine, Columbus, OH 43210.

[2] Department of Cell Biology, Neurobiology, and Anatomy, Ohio State University College of Medicine, Columbus, OH 43210.

[3] Address reprint requests to Donald W. Chakeres, MD, Department of Radiology, Division of Neuroradiology, Ohio State University Hospitals, Ohio State University College of Medicine, 450 W. 10th Avenue, Columbus, OH 43210.

AJNR 14:465–472, Mar/Apr 1993 0195-6108/93/1402-0465

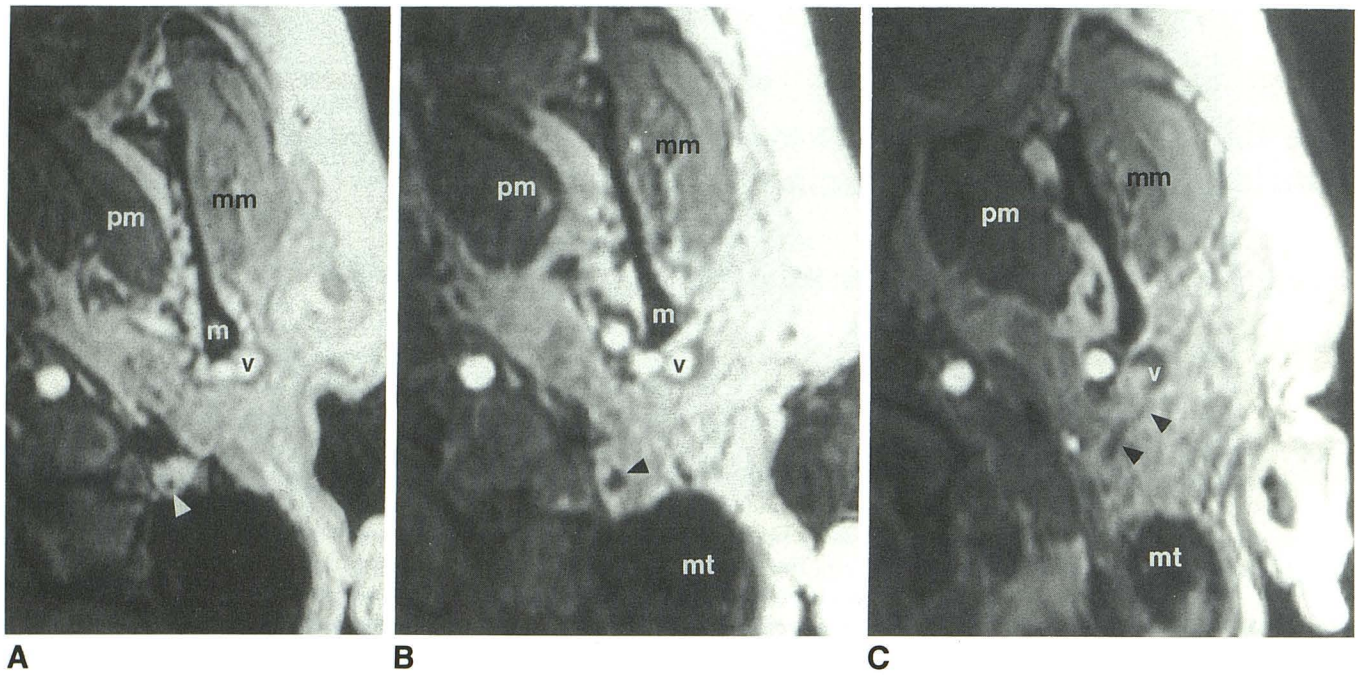

Fig. 1. Normal facial nerve; axial, 3DFT (50/5.3/30) images of the intraparotid facial nerve.

A, The facial nerve (*arrowhead*) is seen within the stylomastoid foramen enveloped by fat. The retromandibular vein (*v*) is seen as a high-signal-intensity structure posterolateral to the mandible. (*pm* = pteryoid muscle; *m* = mandible; mm = masseter muscle).

B, More inferiorly at the level of the mastoid tip (*mt*), the facial nerve (*arrowhead*) is seen along the posteromedial aspect of the parotid gland.

C, Further inferiorly at the level of the mastoid tip (*mt*), the facial nerve (*arrowheads*) courses horizontally and anterolaterally through the parotid gland, lateral to the retromandibular vein (*v*).

tures using previously described 2DFT spin-echo techniques, it can be difficult to differentiate the nerve from a vessel; this distinction can be made only by tracing the course of a structure to see if it follows the typical course of the facial nerve (3). An imaging technique yielding different signal characteristics for vessels and for the facial nerve would simplify this differentiation. This is especially true if the normal course of the nerve is altered by the presence of a mass. An additional advantage of 3DFT over 2DFT techniques is the ability to produce high-quality computer reformations in orthogonal, oblique, or curved planes. These reformations can be extremely helpful in evaluating the complex anatomy in this region and eliminate the need for precise angulation of the original plane of acquisition, as has been described for 2DFT techniques (3).

Our goal, based on the expected advantages described above, was to investigate the use of high-resolution 3DFT gradient-echo MR in evaluation of the extracranial facial nerve.

Materials and Methods

Nine normal volunteers, 22 to 41 years old, and one clinical patient were scanned on a 1.5-T MR system (Signa revision 3.2; General Electric, Milwaukee, WI) (Figs. 1–4). The patient was a 62-year-old man with possible recurrent periauricular basal cell carcinoma. Axial (Fig. 1), sagittal (Fig. 2), and/or coronal high-resolution images were obtained with a 3DFT gradient-echo technique (6, 7) using a standard 3-inch circular surface coil. The examinations were performed with section thicknesses of 0.5 and 1.0 mm, and 28 or 60 sections were obtained. Various fields of view (10, 12, 14, or 16 cm) and matrix sizes (128 × 256 and 256 × 256) were evaluated, thus the voxel sizes ranged from 0.5 × 0.5 × 0.5 mm^3 to 0.6 × 1.2 × 1.0 mm^3.

T1-weighted image contrast was obtained by using a repetition time (TR) of 50 msec, 30° flip angle, and strong spoiler gradients (8). Various echo times (TE) ranging from 4.8 to 9 msec were evaluated (Fig. 3). The minimal possible TE varied depending on the selected spatial resolution. In addition, gadolinium-enhanced images (0.1 mmol/kg) were compared with noncontrast images in three volunteers. Under these conditions, acquisition times ranged from 6:50 to 13:40 minutes.

Orthogonal, oblique, and curved oblique reformatted images were generated in selected cases from original axial, coronal, or sagittal images on a CAMRA S-200 independent imaging workstation (I.S.G. Technologies, Inc, Mississauga, Ontario, Canada) (Fig. 5). The curved oblique images were constructed by manually defining the course of the facial nerve on axial images.

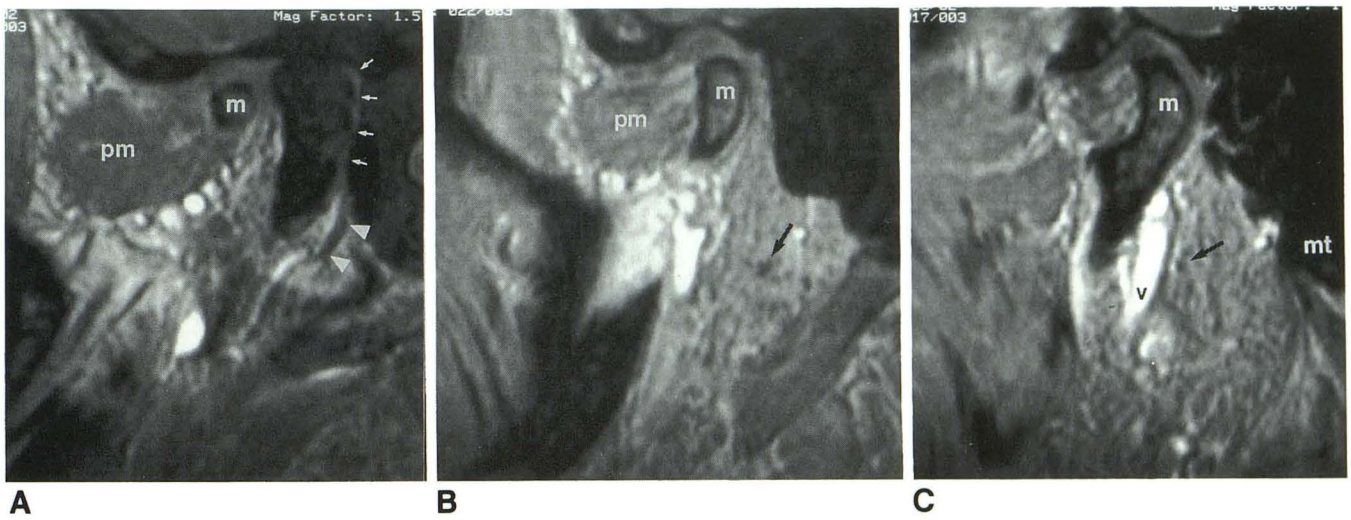

Fig. 2. Normal facial nerve; sagittal, 3DFT (50/5.3/30) images of the intraparotid facial nerve.

A, The posterior genu and descending segments of the facial nerve (*small arrows*) are seen within the temporal bone. The subtemporal segment of the low signal facial nerve (*arrowheads*) within the stylomastoid foramen is enveloped by high signal intensity fat. The pterygoid muscle (*pm*) and medial margin of the mandible (*m*) are seen.

B, Several millimeters laterally, the facial nerve (*arrow*) is seen en face coursing laterally through the posterior aspect of the parotid gland.

C, Most laterally, at the level of the mastoid tip (*mt*), a small intraparotid branch of the facial nerve (*arrow*) is seen en face posterior to the high signal retromandibular vein (*v*).

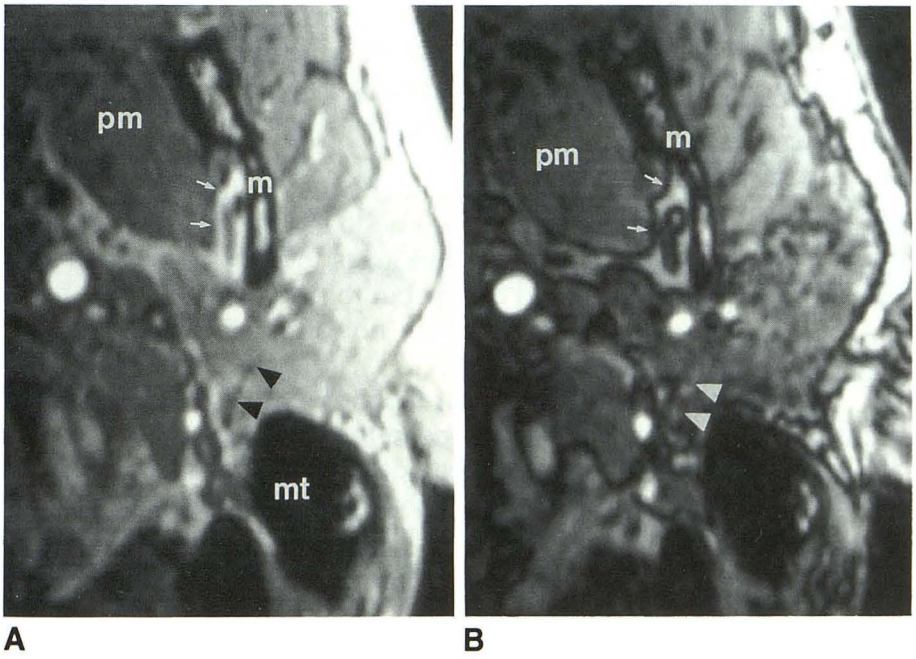

Fig. 3. Variable TE; axial 3DFT images at the level of the mastoid tip (*mt*).

A, 50/5.3. At TE 5.3 msec, fat and water spins are predominantly in phase and summate, increasing the overall signal of the parotid gland and diminishing the artifact at fat-water interfaces (*arrows*). The facial nerve (*arrowheads*), mandible (*m*), and pterygoid muscle (*pm*) are shown.

B, 50/7. At TE 7 msec, fat and water spins are predominantly out of phase and cancel, lowering the overall signal of the parotid gland and accentuating the artifact present at fat and water interfaces (*arrows*) and decreasing the contrast between the facial nerve (*arrowheads*) and the surrounding parotid gland.

Results

Optimization of Imaging Parameters

Axial (Fig. 1), sagittal (Fig. 2), and coronal 3DFT images were obtained. These provided clear information about the course and appearance of the facial nerve, but the axial images were best for showing the overall relationship of the nerve to the parotid gland, vessels, mandible, and adjacent muscles.

With the thinnest section thickness used (0.5 mm), the images had a grainy appearance, with poor definition of the facial nerve due to excessive background noise. A section thickness of 1.0 mm was felt to be optimal with the current hardware and pulse sequence.

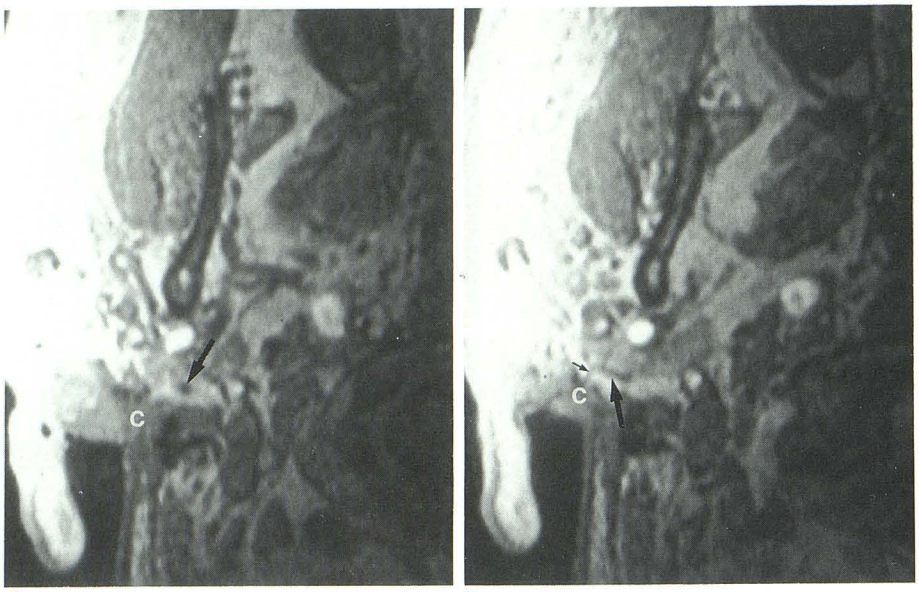

Fig. 4. Recurrent basal cell carcinoma; axial 3DFT images (50/5.3/30). This 62-year-old man had a history of a Moh procedure 2 years earlier for a right periauricular basal cell carcinoma. He presented with progressive skin thickening posterior to the pinna. No facial nerve dysfunction was present, but the relationship of the tumor to the facial nerve needed to be evaluated for presurgical planning.

A, This axial image just below the mastoid tip clearly shows a small amount of high-signal-intensity fat separating the low-signal facial nerve (*arrow*) from a posteriorly located plaque-like area of intermediate signal skin thickening representing recurrent basal cell carcinoma (*c*).

B, Slightly inferiorly, the low signal facial nerve (*large arrow*) is seen coursing in a lateral direction and bifurcating. The small posterior branch (*small arrow*) extends into the intermediate signal carcinoma (*c*). These images accurately predicted the relationship of the facial nerve to the tumor, simplifying the surgical procedure.

Both 28- and 60-section acquisitions were useful. The 28-section acquisitions showed overall higher signal in the venous structures, related to less saturation effects. The advantages of the 60-section acquisition were a larger area of examination (6 cm vs 2.8 cm) and slightly better signal-to-noise ratio.

The optimal field of view was determined to be 12 cm. Fields of view smaller than this had more severe wrap-around (aliasing) artifacts. In addition, with a smaller field of view, accurate positioning of the surface coil became more critical and it is possible that portions of a mass, if present, could be excluded. Larger fields of view provided less spatial resolution.

The optimal matrix with the current pulse sequence was 128 × 256. The 256 × 256 matrix required the use of a longer TE (7 msec), thus yielding decreased contrast. Truncation artifacts related to the air-skin interface were not seen in the region of the facial nerve.

For the same voxel size, both increasing the number of excitations and acquiring 60 rather than 28 sections increases the signal-to-noise ratio. Thus, when 28 sections were acquired, two excitations were usually used. When 60 sections were acquired, one excitation was sufficient for delineation of the facial nerve within the parotid gland. The required total acquisition time (6:50 minutes) is the same with either technique.

Various TEs ranging from 4.8 to 9 msec were evaluated. A TE of approximately 5 msec provided the best images, with higher signal-to-noise and no fat-water interface chemical shift subtraction artifacts (Fig. 3A). With a TE of approximately 7 msec, image contrast was poor. Low signal lines at the interfaces of fat and water structures were present (Fig. 3B). The facial nerve could not be easily delineated from the surrounding parotid gland.

Flow compensation was not used to maintain as a short a TE as possible, maximizing the signal-to-noise ratio. This leads to artifacts from flow in the carotid artery, but for the very short TE used, smaller arteries are not affected by flow-related artifacts.

The administration of Gd-DTPA showed no significant change in the appearance of the facial nerve. However, gadolinium-enhanced images demonstrated slightly higher signal intensity of the veins.

Overall, the optimal exam with the existing hardware and pulse sequence was axial 1-mm-thick images using TR of 50, TE of 5.3 msec, and a 30° flip angle. We used one or two excitations and a 12-cm field of view for this technique. A matrix of 128 × 256 with 28 or 60 sections without gadolinium was used (Fig. 1), yielding a voxel size of 0.5 × 1.0 × 1.0 mm^3. Acquisition time using this optimal technique was 6:50 minutes. A long segment (2–3 cm) of the proximal extracranial facial nerve could be followed on contiguous images in all five volunteers in whom this optimal technique was used.

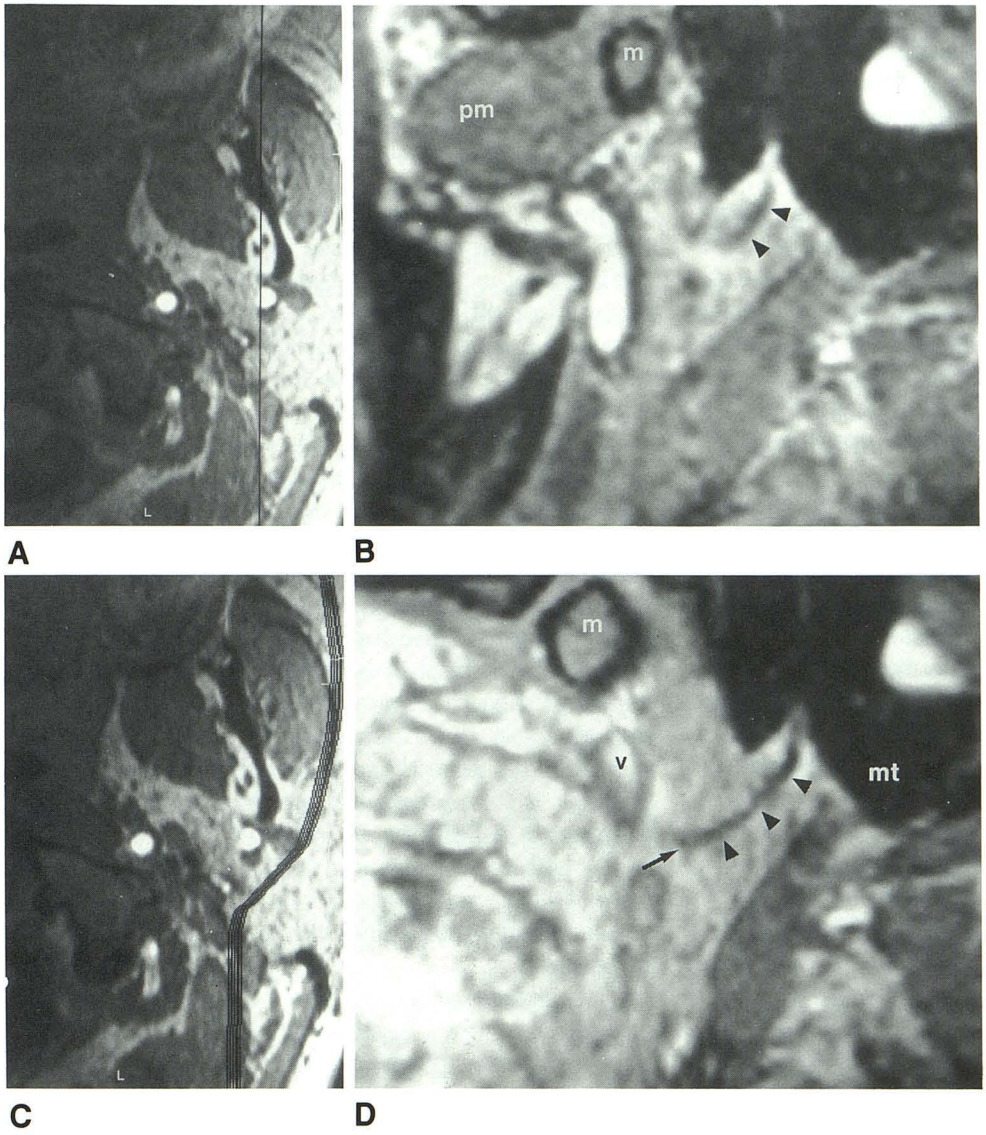

Fig. 5. Reformatted images from axial 3DFT (50/5.3/30) acquisition.

A, This axial image from original acquisition shows the plane of sectioning (*straight black line*) of reformatted sagittal image in *B*.

B, On this reformatted sagittal image, the low-signal-intensity facial nerve (*arrowheads*) is seen in the high-signal-intensity fat of the subtemporal space. Note the similarity in appearance of the nerve, pterygoid muscle (*pm*), and mandible (*m*) in this image as compared to the image originally acquired in a sagittal plane in Figure 2A.

C, This axial image from the original acquisition shows the curved plane of sectioning (*black lines*), which follows the course of the facial nerve, used to produce the image in *D*.

D, A long uninterrupted segment of the facial nerve (*arrowheads*) is seen on this reformatted curved oblique image, extending from the stylomastoid foramen through the subtemporal space and far into the superficial parotid gland. A bifurcation of the nerve is seen distally (*arrow*). The mandibular condyle (*m*), mastoid tip (*mt*), and high-signal-intensity retromandibular vein (*v*) are also seen.

Appearance of the Facial Nerve

The facial nerve was consistently seen using the optimal technique described above as two primary segments, a proximal vertically oriented subtemporal segment, and a distal, oblique, branching intraparotid segment.

As the facial nerve exits the skull base at the stylomastoid foramen (Fig. 1A), it is seen as a hypointense tubular structure, surrounded by the hyperintense fat within the subtemporal space (Figs. 1B and 2A). The apparent diameter of the main trunk of the facial nerve is 1 to 3 mm. On sagittal and coronal images, this proximal vertically oriented segment could usually be seen in its entirety on one or two images. As the nerve enters the high-signal-intensity parotid gland along its posteromedial margin, the second characteristic segment begins as the nerve abruptly angles laterally and anteriorly (Figs. 1C, 2B, and 2C). This intraparotid segment of the nerve ramifies into a variable number of smaller branches, coursing laterally, superiorly, and inferiorly. The number and length of branches seen varies from one subject to another. A characteristic major branch, corresponding to the temporofacial branch, was seen in most studies coursing laterally, then curving anteriorly lateral to the mandible and towards the lateral surface of the masseter. A long, linear segment of this branch was seen on a single axial image in most studies (Fig. 1C). This branch travelled superficial to the retromandibular vein and external carotid artery, coming in close proximity to the vein. The entire extracranial facial nerve was usually seen on 10 to 20 contiguous axial images.

The parotid gland was intermediate in signal in all volunteers, lower in signal than the subcutaneous fat, but higher in signal than the masseter

and other muscles. The parotid gland shows varying degrees of signal inhomogeneity. Vessels were generally seen as high-signal structures in in-flow regions related to time-of-flight phenomena. Saturation effects caused variable loss in signal within the vessels.

In the clinical patient, a plaque-like mass was seen along the skin surface in the retroauricular region (Fig. 4). This mass extended within 1 to 2 mm of the clearly visualized main facial nerve trunk, but did not touch or surround the nerve. A small branch of the nerve could be seen extending into the tumor. The relationship of the recurrent tumor to the nerve was confirmed at surgery.

Orthogonal, oblique, and curve oblique sagittal reformations were produced from some 3-D sets of axial images and were very helpful in confirming the course of the facial nerve and its relationship to adjacent structures. These reformations were overall of nearly equivalent quality to the original images (Figs. 5B and 5D). The curved oblique sagittal images were best at showing the longest segment of the nerve on a single image (Fig. 5D).

Discussion

Because the facial nerve is small and follows a complex course, it is important to use the optimal imaging technique if the nerve is to be seen (9, 10). It is crucial to optimize imaging parameters to obtain the highest quality images. The use of a 3DFT technique as opposed to conventional 2DFT spin-echo techniques was very useful for several reasons. This technique allowed the acquisition of 1-mm-thick sections, four times thinner than with traditional 2DFT spin-echo pulse sequences that have been reported (3). Using this high-resolution 3DFT technique, seven times as many sections can be obtained in a given volume than is possible using previously reported 2DFT spin-echo techniques (3). This higher resolution provides much more precise information about the relationship of the nerve to adjacent structures. Satisfactory visualization of the facial nerve using previously described 2DFT spin-echo techniques required precise angulation of the imaging plane that needed to be identified from initial "scout" images (3). Furthermore, an additional acquisition to provide slightly overlapping sections was required when contiguous sections were necessary. High-quality orthogonal, oblique, and curved reformatted images can be produced after scanning using this high-resolution 3DFT technique because of the method of acquisition, the small section thickness and no intersection gap.

It is also easier to distinguish the facial nerve (which is low signal intensity on both 2DFT T1-weighted images and the 3DFT technique described in this article) from vessels using this 3DFT technique. Because most vessels are hyperintense in certain regions using the 3DFT technique, differentiating vessels from the facial nerve is easier than on 2DFT spin-echo images, on which the vessels are seen as low-signal foci, similar to the facial nerve.

Truncation artifact, which can cause linear areas of low signal intensity that could be confused with the facial nerve, has been reported as a possible pitfall in MR imaging of the extracranial facial nerve (3). Using the technique described in this article, truncation artifact was not observed in the region of the facial nerve.

We found axial images to be overall the most useful of the orthogonal images, because the axial images best demonstrated the entire course of the facial nerve and its relationship to surrounding structures. The number of excitations chosen represents a balance of improved signal-to-noise ratio, but longer imaging time with increasing number of excitations. The number of sections chosen primarily reflects the size of the area to be imaged.

The choice of voxel size (which is a function of field of view, section thickness, and matrix size) represents a compromise between increased spatial resolution and decreased signal-to-noise. A smaller voxel size provides increased spatial resolution at the expense of decreased signal-to-noise. Although we were able to obtain sections thinner than 1 mm and fields of view of less than 12 cm, these images were suboptimal, related to decreasing signal-to-noise ratio. In addition, a smaller field of view can produce greater problems with wraparound artifacts and requires more precise surface coil positioning.

TE has a profound effect on gradient-echo images, in part because fat and water can be in phase or out of phase, depending on TE (Fig. 3) (11). Because fat protons and water protons are in different microscopic environments, they precess at slightly different frequencies. Depending on the TE used, fat and water protons may be in phase or out of phase, related to differences in chemical shift and magnetic field strength. With a 1.5-T field strength, fat and water are out of phase with a TE of 7 msec, causing subtraction

of signal in voxels containing both water and fat. Because the parotid gland is a mixture of fatty and soft-tissue components, there is decreased signal within the gland, making differentiation of the relatively low-signal nerve from the gland more difficult. Thin low-signal margins may also be seen at the interfaces of fatty tissue with predominantly water-containing structures, related to the same phenomenon. With a TE of 4.5 msec, fat and water protons are in phase, thus yielding higher signal for tissues containing both fat and water.

The use of gadolinium had no significant advantages in the evaluation of normal volunteers. Significant enhancement of the normal facial nerve was not observed, although gadolinium did provide increased signal within venous structures. Gadolinium with fat saturation might be useful in evaluating parotid masses, inflammatory or neoplastic abnormalities of the facial nerve, or other pathologic processes in this region.

There are several limitations to this technique. Although the acquisition time compares favorably with previously described techniques, some patients have difficulty remaining still for this length of time. Because very small structures are being evaluated, slight patient movement can cause significant image degradation. Shorter scan times may be achieved in the future by using shorter TRs in combination with radio frequency spoiling rather than gradient spoiling. The method described in this report allows evaluation of only one facial nerve and parotid gland at a time. While this is adequate in most situations, if a process is bilateral (as Warthin tumors may be), simultaneous evaluation of both sides would be beneficial. Specially designed bilateral phased array surface coils and a larger field of view and matrix would be necessary in this case. The optimal method for displaying the images is not yet clear. Because the facial nerve follows a very complex course, most images show only small segments of the nerve or its branches. The smaller branches can be difficult to connect visually to the larger branches from which they originate. At present, viewing images from these exams in rapid sequence on a monitor is helpful in delineating the course of the nerve. In addition, imaging workstations can be useful, both for the simultaneous viewing of orthogonal images on a monitor and for producing various reformatted images as illustrated. 3-D projection images, planar reformations, or surface reconstruction might be useful in displaying the entire nerve and its relationship to adjacent structures, but may require improved contrast and/or higher spatial resolution.

At our institution, we are now using the 3DFT technique described in this paper as our standard protocol when detailed evaluation of the parotid gland and extracranial facial nerve is required. This technique is not meant to be used as a survey exam. The most important role for this imaging technique may be in the preoperative evaluation of parotid masses. This 3DFT technique promises to provide detailed direct information on the location of the facial nerve relative to local pathology, and to demonstrate the distortion and location of major vessels (including the retromandibular vein and the external carotid, internal maxillary, superficial temporal, and occipital arteries), muscles, the parotid duct, the mandible, and other structures in the region. Because there can be considerable variation in the relationship of these structures to the facial nerve, especially when a mass is present, this type of detailed anatomy is very important in presurgical planning. Other possible indications include evaluation for facial nerve neoplasms or perineural spread of extrinsic neoplasms along the facial nerve, traumatic facial nerve injury, infection in the parotid space, congenital anomalies, and Bell palsy.

Acknowledgments

We thank Vicky A. Hacker, BSRT, and Mark Smith, BSRT, MS, for technical assistance; Christian Head, BS, for cadaver dissection; John Croyle, BA, for photography; and Linda Chakeres for editorial assistance.

References

1. Chakeres DW, Kapila A. Normal and pathologic radiographic anatomy of the motor innervation of the face. *AJNR* 1984;5:591–597
2. Brogan MA, Chakeres DW. Computed tomography and magnetic resonance imaging of the normal anatomy of the temporal bone. *Semin Ultrasound CT MR* 1989;10:178–194
3. Teresi LM, Kolin E, Lufkin RB, Hanafee WN. MR imaging of the intraparotid facial nerve: normal anatomy and pathology. *AJR* 1987; 148:995–1000
4. Teresi LM, Lufkin RB, Wortham DG, Abemayor E, Hanafee WN. Parotid masses: MR imaging. *Radiology* 1987;163:405–409
5. Wortham DG, Teresi LM, Lufkin RB, Hanafee WN, Ward PH. Magnetic resonance imaging of the facial nerve. *Otolaryngol Head Neck Surg* 1989;101:295–301
6. Schmalbrock P, Yuan C, Chakeres DW, Kohli J, Pelc NJ. Volume MR angiography: methods to achieve very short echo times. *Radiology* 1990;175:861–865
7. Brogan M, Chakeres DW, Schmalbrock P. High-resolution 3DFT MR imaging of the endolymphatic duct and soft tissues of the otic capsule. *AJNR* 1991;12:1–11

8. Wood ML, Runge VM. Artifacts due to residual magnetization in three-dimensional MRI. *Med Phys* 1988;15:825–831
9. May M. Anatomy of the facial nerve for the clinician. In: May M, ed. *The facial nerve.* New York: Thieme, 1986:21–62
10. Anderson R, Byars L. Anatomy of the parotid area. In: Anderson R, Byars L, eds. *Surgery of the parotid gland.* St. Louis: Mosby, 1965:1–16
11. Wehrli FW, Perkins TG, Shimakawa A, Roberts F. Chemical shift-induced amplitude modulations in images obtained with gradient refocusing. *Magn Reson Imaging* 1987;5:157–158